Journal of Power Sources 243 (2013) 328–335

Contents lists available at SciVerse ScienceDirect

Journal of Power Sources

journal homepage: www.elsevier.com/locate/jpowsour

The influence of gas-diffusion layer properties on elevated temperature operation of polymer-electrolyte fuel cells

Robert M. Darling [a,*], Siddique Khateeb [b]

[a] United Technologies Research Center, 411 Silver Lane, East Hartford, CT 06108, USA
[b] UTC Power, 195 Governor's Highway, South Windsor, CT 06074, USA

HIGHLIGHTS

- We study how the diffusion layer affects water behavior in fuel cells.
- High thermal resistance drives water to cathode and lowers humidity.
- High mass-transport resistance drives water to anode and raises humidity.
- Simple model supports experimental findings.

ARTICLE INFO

Article history:
Received 11 March 2013
Received in revised form
3 June 2013
Accepted 4 June 2013
Available online 13 June 2013

Keywords:
Fuel cell
Water transport
Relative humidity
Heat transfer

ABSTRACT

The performance and water management characteristics of polymer-electrolyte fuel cells depend upon the heat and mass transport properties of the components. The influences of the thermal conductivity and thickness of the cathode gas-diffusion layer on the ability to operate stably over a range of temperatures and relative humidities are investigated in this paper. Low thermal resistance is detrimental at low temperature and beneficial at high temperature. The opposite trends hold for mass transport, although the voltage losses associated with oxygen concentration polarization diminish the benefits of increasing the resistance to mass transport.

1. Introduction

Conventional polymer-electrolyte fuel cells (PEFCs) are sensitive to operating temperature. This sensitivity primarily derives from the state of water in the cell. The water generated by reaction is liquid at low temperatures and vapor at high temperatures. This relationship is depicted in Fig. 1 where the fraction of water leaving the cell as a vapor and the relative humidity of the air and fuel leaving the cell (RH_E) are plotted as a function of coolant temperature. The definition of RH_E is given in the appendix and the conditions are reported in the figure caption. All water exits as vapor above 78 °C; 99% of the water exits as liquid at 1 °C. Liquid water tends to saturate porous media and impede reactant transport to catalyst sites at low temperature. Conversely, Ohmic losses associated with the ionomer in the membrane and catalyst layers tend to be highest at high temperature and low humidity. This conflict makes maximizing performance over a broad range of operating conditions difficult. The relative humidity at a given temperature can be raised by increasing pressure, increasing inlet dew points, or decreasing air flow. However, compressors and water recovery devices add cost and complexity to fuel-cell systems [1]. Restricting air flow can lead to large overpotentials caused by oxygen concentration polarization.

This paper focuses on how the thermal and mass-transport resistances of the gas-diffusion layer (GDL) on the cathode side affect water movement at elevated temperatures and how this affects performance. A conventional GDL consists of carbon fiber paper (CP) coated with poly(tetrafluoroethylene) (PTFE). A typical CP is approximately 190 μm thick and >70% porous with 7 μm diameter fibers and 10–30 μm diameter pores. Graphitized binder material is also present in many CPs. A microporous layer (MPL) containing carbon particles and PTFE usually separates the CP from the catalyst layer. A typical MPL is less than 50 μm thick with 100–500 nm diameter pores [2]. This range of pore sizes corresponds to the transition between ordinary and Knudsen diffusion at atmospheric pressure.

* Corresponding author. Tel.: +1 860 610 7495; fax: +1 860 998 9489.
E-mail addresses: darlinrm@utrc.utc.com, darling888@hotmail.com (R.M. Darling).

0378-7753/$ – see front matter © 2013 Elsevier B.V. All rights reserved.
http://dx.doi.org/10.1016/j.jpowsour.2013.06.015

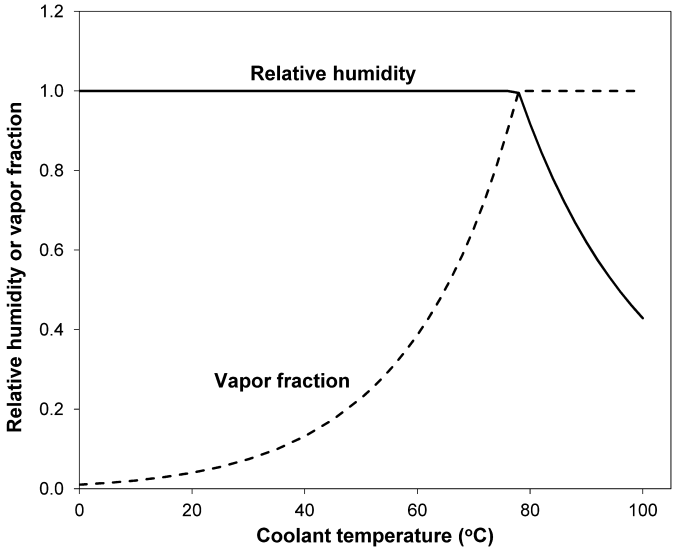

Fig. 1. Relative humidity and vapor fraction as a function of coolant temperature. Fuel: 170 kPa, 1.2× stoichiometric flow, 53 °C dew point. Air: 170 kPa, 1.5× stoichiometric flow, 0 °C dew point.

The combined influence of thermal and mass-transport properties on water vapor movement through the GDL has been described by a number of researchers including Weber and Newman [3], Burlatsky et al. [4], Owejan et al. [5] and Caulk and Baker [6]. These authors convincingly argued that water vapor moves down the temperature gradient in the GDL caused by the heat flux and that vapor transport can dominate even when gases are fully humidified. While the results presented in the cited works are compelling, none includes water distribution measurements or examines the influence of GDL thickness.

The objective of this work is to understand how the transport properties of the CP affect behavior at high temperatures. The link between drying of the membrane-electrode assembly and the thermal resistance of the diffusion media has not been explicitly addressed in the publications cited above. This issue is explored in this work by augmenting the model presented by Caulk and Baker [6] with a relative humidity calculation that describes the hydration state of the membrane-electrode assembly. Predictions for fully humidified and sub-saturated conditions quantify how the properties of the CP influence the range of temperatures yielding stable operation. The predicted operating regimes are qualitatively compared to experimental data from cells with CPs having different thermal conductivities and thickness. In particular, the veracity of the model is interrogated by qualitative comparison to voltage–temperature responses at fixed current and measured water distributions between air and fuel.

2. Mathematical model

Fig. 2 shows a schematic diagram of the region of interest, which consists of the flow field, diffusion media, and catalyst layer on the cathode side of a PEFC. Temperature and relative humidity are specified at the flow-field (FF) boundary on the left. The relative humidity at the FF is set to RH_E in this work. Water flux, n_w, and heat flux, q, are specified at the cathode catalyst layer (CL) boundary on the right. The primary result is RH_{CL}. Heat and vapor transport are solved in the direction perpendicular to the membrane through the composite diffusion medium consisting of CP and MPL. The carbon paper contacts ribs that are separated by gas channels in conventional PEFCs; this detail is not shown in the diagram. Ribs

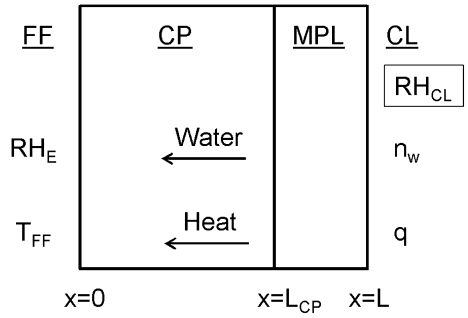

Fig. 2. Schematic diagram of region of interest showing temperature at the flow field, T_{FF}, and exiting relative humidity, RH_E, as boundary conditions at the flow field on the left. The water flux, n_w, and heat flux, q, are specified at the catalyst layer on the right. The relative humidity at the catalyst layer, RH_{CL}, is the main result.

and channels are typically wider (~1 mm) than the thickness of the diffusion media (~200 μm), suggesting that two dimensional effects in the plane of the membrane may be important. Caulk and Baker, however, showed good agreement between predicted and measured dry to wet transitions using a one-dimensional model for heat and mass transport essentially identical to the one discussed in this work [6]. Therefore, a one-dimensional approach that uses composite rib/channel boundary conditions yields a good first approximation. Weber discussed a method for calculating an effective one-dimensional length for a GDL confined by ribs and channels [7]. Variations over the active area and transients are ignored as well. Qualitative comparison of the model to experimental data is appropriate given these approximations.

Temperature and vapor pressure profiles through the diffusion media were determined using the formulation presented by Caulk and Baker [6] with minor modifications. Complete derivations are not repeated here, instead we simply present the equations used to calculate the relative humidity in the catalyst layer, and the fraction of water exiting via the cathode. The influence of thermal conductivity on operation at low temperature has been presented before as mentioned in the introduction; however the results of these calculations are included here in order to clarify the nature of the trade between hot and cold performance arising from the selection of a particular set of materials.

Heat conduction through the CP and MPL is assumed to follow Fourier's law, and heat flux is assumed to be continuous across all boundaries. All heat is assumed to flow through the solid phase, in view of the relatively low thermal conductivity of gases. Heat generation in the diffusion media by IR is neglected. Furthermore, no attempt is made to account for enthalpy changes due to evaporation or condensation of water in the diffusion media. A thermal contact resistance between the FF and CP is included in the formula for total thermal resistance. The temperature at the catalyst layer is:

$$T_{CL} = T_{FF} + z_H i(E - V)R_t; \quad R_t = R_{t,c} + \sum_i \frac{L_i}{k_i} \tag{1}$$

where T_{FF} is the temperature at the flow field, z_H is the fraction of the heat generated that exits via the cathode, i is the current density, E is the thermo-neutral or enthalpy voltage, V is the cell voltage, R_t is the total thermal resistance, L_i is the thickness of component i, k_i is the thermal conductivity of region i, and $R_{t,c}$ is the thermal contact resistance between the ribs and CP. Index i in Equation (1) includes the MPL and CP. $R_{t,c} = 5 \times 10^{-5}$ W^{-1} m^2 K, taken from Ref. [6]. Caulk and Baker use $z_H = 0.5$ [6], Burlatsky et al. suggest $0.25 < z_H < 0.5$ [4]. In this work, z_H was estimated for the different configurations by assuming that all heat is generated in the cathode catalyst layer (Table 2 in Ref. [3] gives 77.3% with a

Table 1
Thickness and thermal conductivity.

Layer	Thickness (μm)	Thermal conductivity (W m^{-1} K^{-1})	Thermal resistance (10^3 × W^{-1} m^2 K)	Reference
Contact	N/A	N/A	0.05	[6]
Anode carbon paper	200	1.4	0.14	[6]
Anode microporous layer	45	0.057	0.79	[4]
Anode catalyst layer	3	0.27	0.01	[8]
Membrane	25	0.254	0.10	[9]
Cathode catalyst layer	3	0.27	0.01	[8]
Cathode microporous layer	10	0.057	0.18	[4]
Cathode carbon paper	See Table 3			

thicker membrane and a relatively large overpotential on the anode), and that all heat moves by conduction. Applying these approximations yields:

$$z_H = \frac{R_{t,c} + \sum_{anode} L_i/k_i}{2R_{t,c} + \sum_{cell} L_i/k_i} \quad (2)$$

The numerator sums over all components from the anode flow field to the membrane, while the denominator sums over all components. The catalyst layers are very thin and do not contribute much thermal resistance, consequently apportioning a fraction of the thermal resistance of the cathode catalyst layer to the numerator would not strongly affect the results. Table 1 summarizes the thermal properties of the various layers; carbon paper properties are given in Table 3. The final column of Table 3 contains the values of z_H calculated for the different cell configurations considered in this work. These values range from 0.66 to 0.79.

The enthalpy voltage derived from an over all isothermal energy balance is:

$$E = f_v E_v + f_l E_l \quad (3)$$

E_v = 1.253 V and E_l = 1.481 V at 25 °C. The subscripts v and l denote vapor and liquid, respectively. The weak variations of E_v and E_l with temperature are accounted for in this work. While E_v and E_l are nearly independent of temperature, E is not because the vapor and liquid fractions are strong functions of temperature, as depicted in Fig. 1. E approaches E_v at elevated temperatures and E_l at low temperatures. The procedure for calculating f_v and f_l is given in the appendix. Caulk and Baker used $E = E_v$ exclusively, because all of their tests were done at 77% relative humidity.

Table 2
Mass-transport parameters.

Description	Symbol	Value	Source
MacMullin number, carbon paper	$N_{m,CP}$	3.65	[12]
MacMullin number, microporous layer	$N_{m,MPL}$	2.45	Estimated from porosity
Bulk diffusivity of water in air	D_i	0.39 cm^2 s^{-1}	At 80 °C, 1 bar.
Hydraulic diameter	L_{FF}	0.52 mm	Design
Rib coverage	r	0.46	Design
Aspect ratio[a]	a	0.35	Design
Nusselt number	Nu	4.128	[11]
Lewis number correction	$Le^{1/3}$	1.04	Calculated (80 °C, 1 bar)
Sherwood number	Sh	4.290	Calculated (80 °C, 1 bar)

[a] Channel depth divided by channel width.

Table 3
Carbon paper properties.

Material	Thickness (μm)	MacMullin number	Thermal conductivity (W m^{-1} K^{-1})	Thermal resistance (10^3 × W^{-1} m^2 K)	Fraction of heat leaving via cathode
Toray 30	100 ± 10	3.65	1.4	0.07	0.79
Toray 90	300 ± 10	3.65	1.4	0.21	0.71
GDL-A	100 ± 10	3.65[a]	0.3	0.33	0.66

[a] Assumed.

Fick's law is used to describe transport of water vapor through the diffusion media. The influence of counter diffusing oxygen is neglected, and convection within the diffusion media is ignored. The partial pressure of water in the catalyst layer is not allowed to exceed the saturated vapor pressure evaluated at the temperature of the catalyst layer. Thus,

$$p_{w,CL} = \min\{p_{sat}(T_{CL}),\ RH_E \cdot p_{sat}(T_{FF}) + \Delta p_w\} \quad (4)$$

$$\frac{\Delta p_w}{RT} = \frac{z_w i R_{mt}}{2F};\ R_{mt} = \frac{L_{FF}(1+r)}{Sh \cdot D_{FF}} + \sum_i \frac{N_{m,i} L_i}{D_i} \quad (5)$$

where $p_{sat}(T)$ is the saturated vapor pressure of water at temperature T, p_w is the partial pressure of water, R is the universal gas constant, z_w is the fraction of product water that exits via the cathode, R_{mt} is the total resistance to mass transport, F is the Faraday constant, D_i is the bulk diffusion coefficient of water vapor through air in region i, $N_{m,i}$ is the MacMullin number, a ratio of bulk to effective diffusion coefficients, in component i, L_{FF} is the hydraulic diameter of the flow channels, r is rib width divided by the sum of rib plus channel width, and Sh is the Sherwood number. The summation includes the CP and MPL. The factor of $1 + r$ corrects for expansion in area from the channel to the electrode. The Sherwood number is related to the Nusselt number by the expression: $Sh = Nu \cdot Le^{1/3}$ (see Ref. [10], for example). The Lewis number, a ratio of thermal to mass diffusivity, is approximately 1 for gases. Nu = 4.128 was calculated using an expression given by Dharaiya and Kandlikar [11] (their Equation (13)) for heat transfer under fully developed laminar flow in a rectangular channel with three insulating walls and a constant heat flux on the fourth wall. Table 2 summarizes the mass-transport parameter values used in this paper. Martinez et al. reported $2.08 \le N_m \le 4.69$ for various CPs, with a value of 3.65 for Toray 60 [12]. Caulk and Baker used values ranging from a low of 2.2 to a maximum of 3.8 for Toray 60. Ordinary diffusion was assumed to prevail in the MPL for lack of specific information regarding pore diameter. This is usually an acceptable assumption [13].

For ordinary diffusion, D_i is inversely proportional to total pressure and increases approximately as $T^{2.334}$ for water paired with a non-polar gas [14]. The saturated vapor pressure was calculated with Antoine's equation:

$$\ln p_{sat} = A - B(T + C)^{-1} \quad (6)$$

with $A = 11.6832$, $B = 3816.44$, $C = 227.02$, with T in K and p_{sat} in bar [15]. The density of the gas varies modestly over the temperature range explored in this work; therefore $T = T_{FF}$ is used in the denominator of the left side of Equation (5), and D_i is evaluated at T_{FF} for all regions.

The relative humidity at the catalyst layer is:

$$RH_{CL} = \frac{p_{w,CL}}{p_{sat}(T_{CL})} \quad (7)$$

$RH_{CL} \leq 1$ because $\max\{p_{w,CL}\} = p_{sat}(T_{CL})$ by Equation (4). Increasing RH_{CL} above RH_E is desirable at hot, dry conditions where $RH_E < 1$. This can be accomplished by increasing resistance to vapor transport to raise $p_{w,CL}$ or decreasing thermal resistance to lower T_{CL}. Increasing the resistance to vapor transport to raise the humidity in the catalyst layer reduces oxygen access. Therefore, this approach is narrowly applicable. Unfortunately, reducing the temperature rise across the CP negatively affects water removal via the vapor phase at low temperatures when $RH_E = 1$ [5].

The fraction of water that can be transported from the cathode catalyst layer to the flow field as vapor without condensing is:

$$z_w = \frac{2F\left(p_{sat}(T_{CL}) - p_{w,FF}\right)}{RTiR_{mt}} \approx \frac{2z_H F(E-V)R_t}{RTR_{mt}}\left(\frac{\partial p_{sat}}{\partial T}\right)_{T_{FF}} \quad (8)$$

$p_{sat}(T_{CL})$ is evaluated at the catalyst layer temperature determined from Equation (1). All calculations were done with the first expression. The second expression, which is found by linearizing the partial pressure profile, shows how z_w depends on thermal and mass-transport resistances explicitly. Burlatsky et al. calculated z_w in a similar manner, while Caulk and Baker assumed that z_w was constant and equal to 1. An upper limit of $z_w = 1$ is enforced in this work.

Fig. 3 shows predicted relative humidity at the catalyst layer as a function of temperature when z_w is maintained at a constant value of 1 for the carbon papers listed in Table 3. Other material parameters are listed in Tables 1 and 2. RH_E, which nearly overlays RH_{CL} for GDL-A, is given for the sake of comparison. These calculations were done for dry air fed at 1.5× the stoichiometric flow and 170 kPa absolute pressure, and hydrogen with a dew point of 53 °C fed at 1.2× the stoichiometric flow and 170 kPa. The cell voltage was 0.6 V, and the current density was 1.3 A cm^{-2}. RH_{CL} increases with increasing transport resistance and decreasing thermal resistance. The resistances of 25 μm thick, 1100 equiv weight Nafion membranes (N211) in equilibrium with RH_{CL} for the three CPs are plotted against the right vertical axis. The membrane resistance is a convenient indicator of the hydration state of the MEA. However, the voltage decline observed when a cell dries includes important contributions from the catalyst layers as well. Resistance increases markedly as humidity drops. Above 80 °C, resistance decreases with increasing transport resistance and decreasing thermal resistance. The humidity calculations presented here assume constant current and voltage and do not account for the additional heat production caused by the rise in IR. For reference, at 1.3 A cm^{-2} and 0.6 V, a resistance increase of 0.1 Ω cm^2 would increase heat production by 20% when the product is vapor. Thus, voltage will decline more rapidly above $RH_{CL} = 1$ than Fig. 3 suggests.

Fig. 4 shows RH_{CL} as a function of temperature when z_w is set to the fraction of water that can be transported from the cathode catalyst layer to the flow channels as vapor without condensing. This value is calculated with Equation (8). z_w for the three GDLs is plotted against the right vertical axis. The values of RH_{CL} for the different GDLs are much more similar above 80 °C when z_w is allowed to vary than they were when z_w was set to 1 uniformly. Forcing all water to leave via the cathode by setting $z_w = 1$ gives rise to significant differences in water partial pressure and relative humidity at the cathode catalyst layer. Thick Toray 90 retards water movement more than thin Toray 30, for example. Therefore, if the flux of water through the two carbon papers is the same, the water concentration difference will be larger for the thick Toray 90. When z_w is allowed to vary the differences in inherent resistance to mass transport are compensated by differences in flux through the cathode GDL. Less water leaves via the cathode in the case of Toray 90 than for Toray at temperatures near 80 °C. Allowing z_w to vary leads to much smaller differences in resistance and performance between the various GDLs at hot, dry conditions than Fig. 3 would suggest. z_w increases with temperature and reaches a maximum of 1 in all cases. The temperature at which $z_w = 1$ varies from 74 °C for GDL-A to 102 °C for Toray 90. Thus high thermal resistance and low mass-transport resistance favor water movement toward the air stream.

3. Experimental

All tests were done on single cells having an active area of 302 cm^2. Testing was done with large cells at technically relevant conditions instead of with small cells at differential conditions in order to eliminate uncertainties associated with scaling of the experimental results. In particular, specifying appropriate dew points for differential cells intended to simulate portions of a large cell operating at low humidity is not straightforward. It is conceivable that different dew points would be appropriate for simulating the same portion of the active area for cells with different components. Because large cells were selected for this study, the one-dimensional model and the experimental data can only be compared qualitatively.

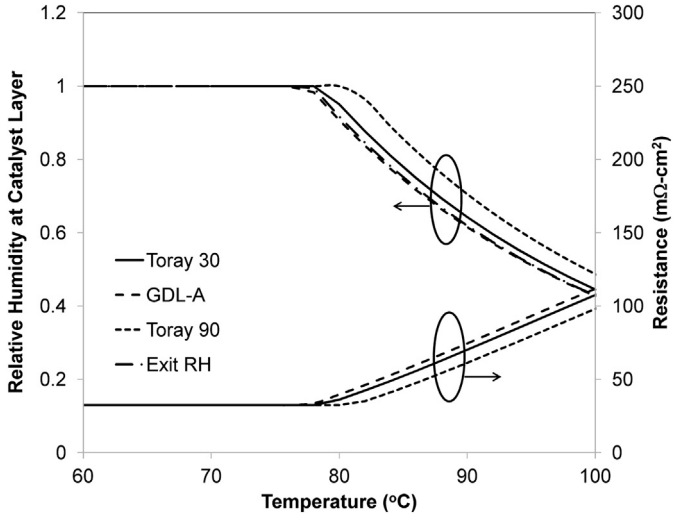

Fig. 3. Relative humidity of catalyst layer as a function of temperature with the fraction of water leaving the cathode, z_w, equal to 1 for all three carbon papers. Conditions are reported in column 3 of Table 5.

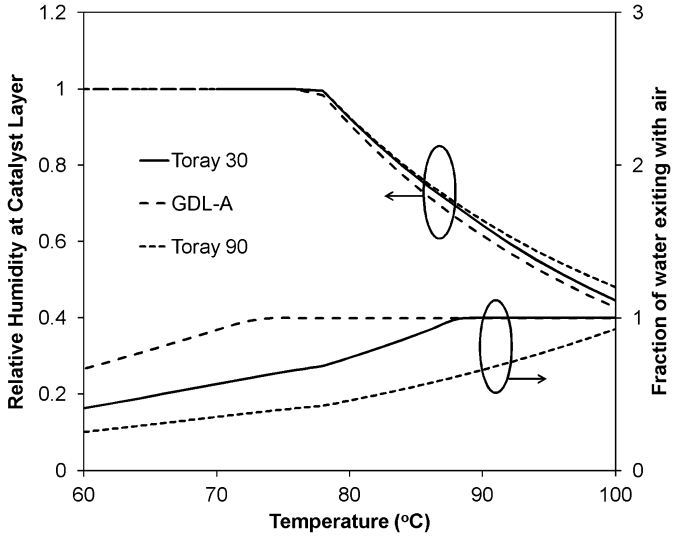

Fig. 4. Relative humidity of catalyst layer as a function of temperature with the fraction of water exiting via the cathode, z_w, equal to the fraction of water that can exit through the cathode GDL without condensing. Conditions are reported in column 3 of Table 5.

Table 3 describes the different cathode carbon papers tested in this work. All papers were dipped in a dispersed Teflon® solution (DuPont FEP 121A) and dried at 180 °C. The final mass fraction of PTFE ranged from 18 to 20 wt%. The first two papers listed in Table 3 have the same intrinsic properties and differ only by thickness. The third paper is from a different supplier and has lower thermal conductivity than the papers from Toray.

A thin MPL containing carbon (Vulcan XC-72, Cabot) and 20 wt% PTFE coated the CP on the cathode. The MPL ink, consisting of 300 g distilled water, 1 g Triton X-100, 10 g carbon, and 2 g dispersed Teflon® (DuPont TE-3893), was mixed in an ice bath with slow addition of carbon and PTFE. The MPL was applied to the CP with a Mayer rod coater running at slow speed. The MPL was then dried in a vacuum oven for 2 h at 40 °C and, subsequently, sintered at 350 °C for 15 min.

Components other than the cathode CP were the same in all cells. Table 4 describes these components. Interdigitated channels were used on the air side; straight, parallel channels were used on the fuel side. Each reactant executed one pass over the active area in opposite directions. Air and coolant flowed in the same direction. A thicker MPL was added to as-received Toray 60 to form the anode diffusion layer. The membrane-electrode assembly consisted of a thin (<30 μm) membrane with in-house platinum on carbon catalyst layers containing 0.1 mg/cm^2 Pt.

The cells were compared with polarization curves and temperature sweeps. The fuel and air pressures and the coolant temperature were controlled exiting the cell. Dew points were set by bubbling fuel and air through hot water.

The water exiting with the fuel and air was collected during a series of tests done to characterize the impact of temperature on water movement. Dry fuel and air were fed while the current density was held at 1 A cm^{-2} for 3 h. The water exiting the cell was condensed and weighed. The masses of water carried by the air and fuel saturated at the trap temperature were added to the liquid to give the total. Greater than 97% of the water generated by reaction was accounted for by this procedure in all cases.

4. Results and discussion

Fig. 5 compares polarization curves for the three cells near $RH_E = 1$. Operating conditions are given in the second column of Table 5. The cells with Toray 30 and GDL-A behave similarly over the entire current density range. The cell with Toray 90 is considerably worse than the others above 1.2 A cm^{-2}. The relatively poor performance at high current is consistent with higher oxygen concentration polarization through the thicker CP. The calculated limiting currents associated with oxygen transport external to the catalyst layer are 10.8 A cm^{-2} for Toray 30 and 4.9 A cm^{-2} for Toray 90 at the average oxygen mole fraction of 0.12. Significant oxygen transport losses are expected to occur in the air electrodes because they contain just 0.1 mg/cm^2 Pt (see Ref. [16] for example). Including a limiting current density of 4 A cm^{-2} associated with diffusion through ionomer in the catalyst layer in both cases reduces these limiting current densities to 2.92 and 2.20 A cm^{-2}, respectively.

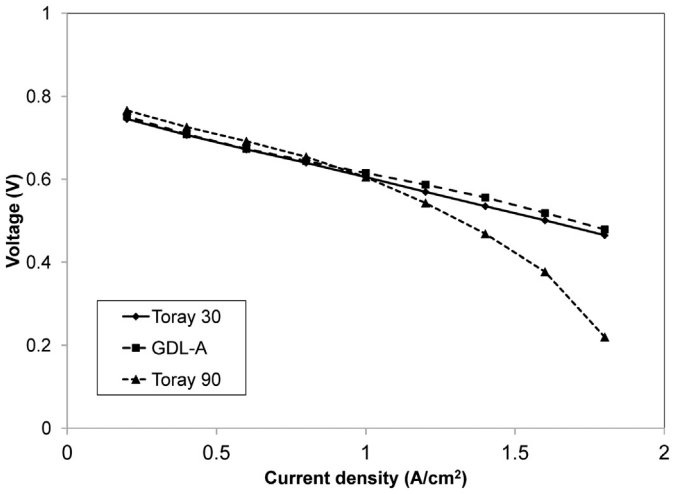

Fig. 5. Polarization at an exiting relative humidity of 0.95 for the cells with Toray 30, GDL-A, and Toray 90 cathode carbon papers. Conditions are reported in the second column of Table 5.

Fig. 6 compares the fraction of water leaving with the air stream during the water collection experiments (see the fourth column of Table 5 for conditions) to model predictions. The fraction of water exiting in the air stream increases with increasing temperature for all CPs in proportion to the exponential increase in saturated vapor pressure. Furthermore, z_w decreases with increasing mass-transport resistance and decreasing thermal resistance, as predicted. The agreement between model and experiment is poorest for the thick Toray 90, and could be improved by decreasing mass-transport resistance or increasing resistance to heat transport. A 25% decrease in total mass-transport resistance, not shown, yields good agreement between model and experiment for Toray 90. This adjustment decreases the temperature at which $z_w = 1$ under these conditions from 94 °C to 86 °C.

Fig. 7 shows temperature sweeps at 1.3 A cm^{-2} for the cells with Toray 30 and GDL-A. The cells are otherwise identical. Operating conditions are listed in the third column of Table 5. As a point of reference, $RH_E = 1$ at 78 °C. Above 80 °C, the cell with Toray 30 is distinctly better than the cell with GDL-A. The voltage of the cell with GDL-A deteriorates precipitously above 79 °C. The temperature at which severe voltage losses occur is approximately 3 °C

Table 4
Cell components.

Side	Component	Description
Fuel	Flow field	Straight parallel channels
	Carbon paper	Toray TGP-060
	Microporous layer	Vulcan XC-72 carbon + Teflon
	Catalyst layer	0.1 mg/cm^2 Pt
	Membrane	Not disclosed
Air	Catalyst layer	0.1 mg/cm^2 Pt
	Microporous layer	Vulcan XC-72 carbon + Teflon
	Carbon paper	See Table 3
	Flow field	Interdigitated channels

Table 5
Experimental conditions.

	Polarization curve	Temperature sweep	Water collection
Current density (A cm^{-2})	0.2 to 1.8	1.3	1.0
Fuel			
Stoichiometry	1.2	1.2	1.2
Dew point (°C)	53	53	0
Exit pressure (kPa)	140	170	140
Air			
Stoichiometry	1.5	1.5	1.5
Dew point (°C)	53	0	0
Exit pressure (kPa)	140	170	140
Coolant			
Exit temperature (°C)	80	69 to 95	65 and 75
Flow (cm^3 min^{-1})	300	300	300
Exiting relative humidity	0.95	1.39 to 0.51	1.33 and 0.86

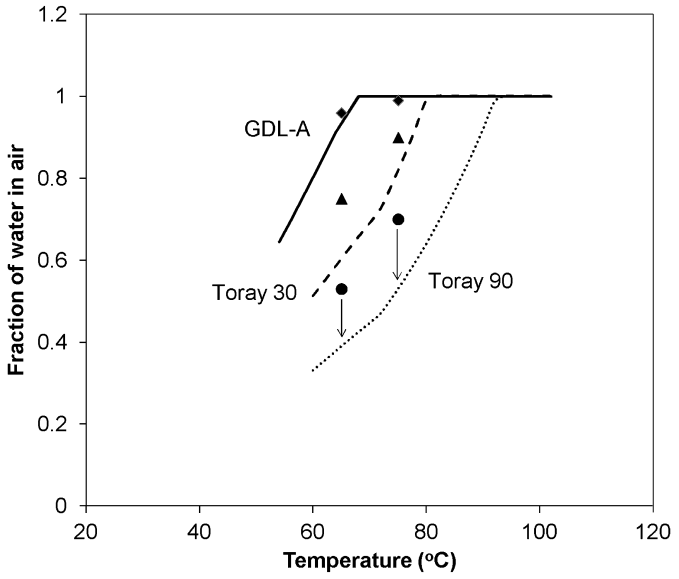

Fig. 6. Measured and predicted fractions of water in air exhaust as a function of temperature for different carbon papers. See the fourth column of Table 5 for conditions.

higher for the Toray 30 cell. The simulations with $z_w = 1$ presented earlier gave a temperature shift ranging from 1.3 °C at $RH_{CL} = 1$– 1.1 °C at $RH_{CL} = 0.4$. The resistances of the cells increase in synchrony with the voltage declines. This supports the contention that decreasing hydration in the membrane-electrode assembly is primarily responsible for the losses. The voltages and resistances of the cells behave in qualitative agreement with predictions from the previous section: high thermal resistance is detrimental at high temperature. The voltage decline is more than double the IR increase for both CPs, indicating that much of the increase in polarization occurs in the catalyst layers.

Fig. 8 shows temperature sweeps for Toray 30 and 90. The cells act similarly for 70 °C < T < 82 °C. The maximum operating temperature increases as the thickness of the CP increases. The benefit of Toray 90 over Toray 30 is approximately 2.5 °C. The predictions with $z_w = 1$ from the preceding section average 2.4 °C for $0.4 < RH_{CL} < 1.0$. Improved high temperature performance with thicker CPs is not predicted to be generally true. The model predicts

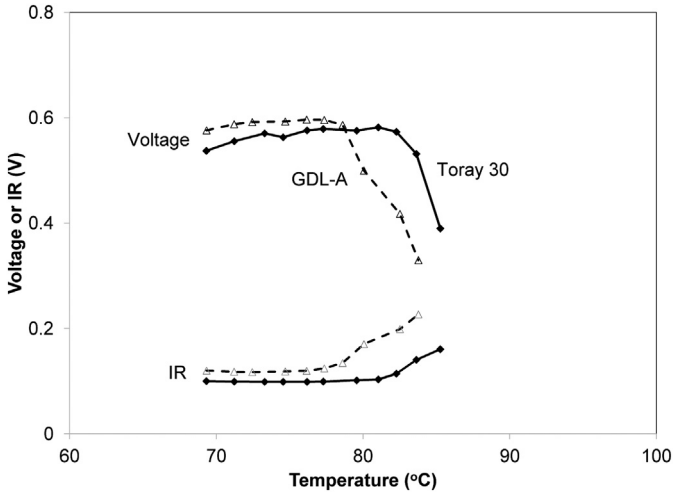

Fig. 7. Temperature sweeps with Toray 30 and GDL-A at 1.3 A cm^{-2}. The exiting relative humidity is 1 at 78 °C. Conditions are given in the third column of Table 5.

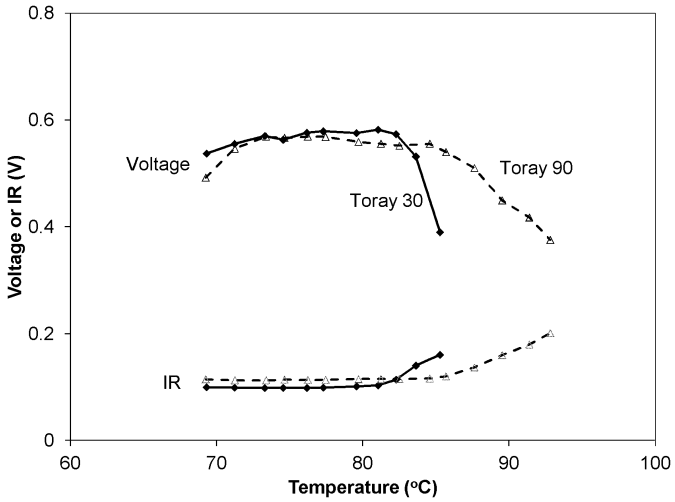

Fig. 8. Temperature sweeps for Toray CPs of different thickness. The exiting relative humidity is 1 at 78 °C. Conditions are given in the third column of Table 5.

that increasing the thickness of a CP with a thermal conductivity of 0.3 W m^{-1} K^{-1} and the same diffusion characteristics would worsen performance slightly at hot, dry conditions. Increasing concentration polarization increases RH_{CL}, while increasing temperature rise decreases RH_{CL}. For Toray 30, the CP accounts for 59% of the resistance to mass transport, and just 24% of the resistance to heat transfer. Conversely, for GDL-A, the CP accounts for 59% of the resistance to mass transport and 60% of the resistance to heat transport. Therefore, increasing the thickness of Toray 30 to add transport resistance raises the total thermal resistance less than increasing the thickness of GDL-A by the same amount would.

Fig. 9 compares measured membrane resistances to resistances predicted with $z_w = 1$ for GDL-A and Toray 90 in the vicinity of $RH_{CL} = 1$. Results for Toray 30, which are intermediate between those shown, were not added to the graph for the sake of clarity. Contact and electronic resistances were subtracted from the measured high-frequency resistances of the cells to obtain the membrane resistance. The agreement between model and

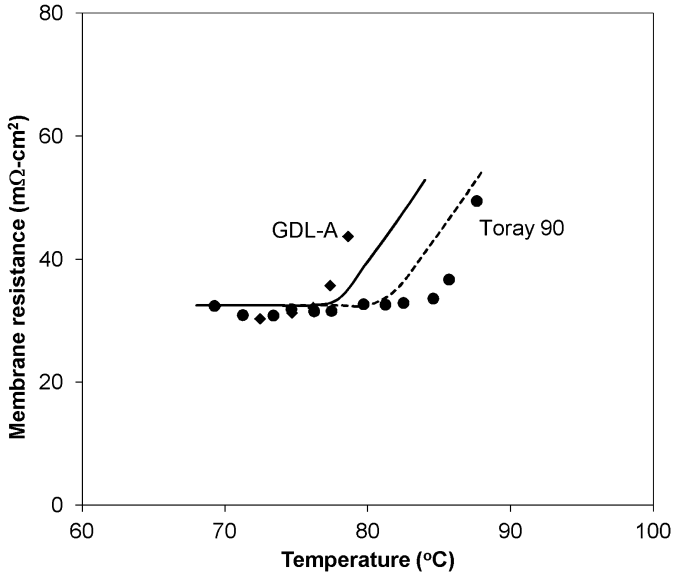

Fig. 9. Measured and predicted membrane resistances for cells with GDL-A and Toray 90 with the fraction of water leaving via the cathode set equal to 1. Conditions are given in the third column of Table 5.

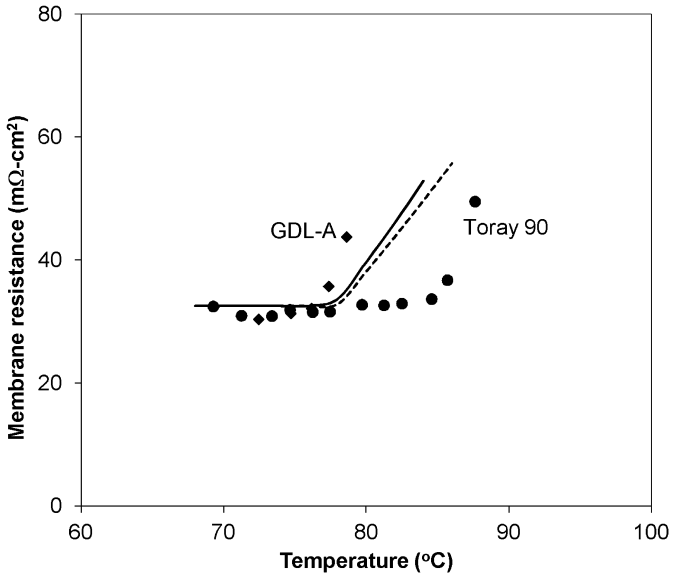

Fig. 10. Measured and predicted membrane resistances for cells with GDL-A and Toray 90 when the fraction of water leaving via the cathode is allowed to vary. Conditions are given in the third column of Table 5.

experiment is not quantitative, but the model captures the influences of mass-transport and thermal resistances on the drying of the membrane as coolant temperature is increased. GDL-A, which has relatively high thermal resistance and low transport resistance, transitions from wet to dry at the lowest temperature. Conversely, Toray 90 transitions from wet to dry at the highest temperature as predicted. The predictions can be shifted to the left by increasing the ratio of thermal resistance to mass-transport resistance; decreasing this ratio shifts the curves to the right.

Fig. 10 compares the data shown in Fig. 9 to resistances predicted when z_w is determined by Equation (8). In this case, z_w is the maximum fraction of water that can exit via the air stream without condensing. The agreement between model and experiment for Toray 90 is considerably worse with variable z_w, suggesting that the calculated value of z_w is too low. This interpretation is consistent with the water balance measurements shown in Fig. 6 which show more water leaving via the cathode than predicted.

5. Conclusions

The influences of the heat and mass transport characteristics of the carbon paper on the cathode side of a PEFC on performance at elevated temperature were studied theoretically and experimentally. Greater resistance to heat transport causes significant dehydration to occur at lower temperature which yields lower performance under hot, dry conditions. This trend opposes the benefit of lower thermal conductivity under cooler, wetter conditions described by other researchers. For materials with high thermal conductivity, a thicker CP on the cathode side improves performance at elevated temperatures. The experimental results are supported by a simple model that predicts how diffusion layer properties affect the amount of water that leaves with the air and the relative humidity in the catalyst layer.

Acknowledgments

This work was supported by United Technologies. The authors are thankful to Bill Bajorek and Jim Brozowski for assistance with experiments.

Appendix A. Exiting relative humidity

An empirical parameter denoted RH_E that describes the relative humidity of a cell is derived in this appendix. This parameter is useful for succinctly correlating trends with air flow, pressure, dew point temperature, and coolant temperature. Correlation with changes in fuel flow is less reliable and depends on the juxtaposition of the fuel and air flow patterns.

The activity of water in the air and fuel streams exiting the cell should be the same if the cell behaves like a single equilibrium stage. Further assuming that the air and fuel streams exit the cell at the same pressure and the coolant exit temperature, allows us to equate the mole fractions of water in the two streams:

$$y_{w,a}(T_c) = y_{w,f}(T_c) \tag{A1}$$

The subscripts a, f, and c refer to the air, fuel, and coolant, respectively. All quantities are evaluated exiting the cell.

The mole fractions of water in the fuel and air exit streams can be calculated by material balance. The material balances are written with all of the water appearing in the gas phase. Thus, the calculated mole fractions of the exit streams can exceed the saturated value. This is indicative of two-phase flow. Combining the total and water mole balances yields:

$$y_w = \frac{N_w}{N_T} = \frac{N_w^0 + \frac{2I}{4F}}{N_T^0 - \frac{I}{4F}} = \frac{y_{w,f}^0 N_f^0 + y_{w,a}^0 N_a^0 + \frac{2I}{4F}}{N_f^0 + N_a^0 - \frac{I}{4F}} \tag{A2}$$

In the above equation, N is molar flow, y is a mole fraction, I is current, and F is the Faraday constant. We have adopted the convention that a variable with a superscript 0 is evaluated at the inlet, while a variable without a superscript is evaluated at the exit. The subscripts are as follows: w = water, T = total, a = air, and f = fuel. The numerator in the second equality shows an increase in number of moles due to water generation by reaction. The denominator in the second equality shows a net loss in moles due to consumption of oxygen and hydrogen.

Dividing through by N_f^0 and introducing utilization and inlet mole fractions of hydrogen and oxygen yields

$$y_w = \frac{y_{w,f}^0 + y_{w,a}^0 \left(\frac{y_{H_2}^0 u_{H_2}}{2 y_{O_2}^0 u_{O_2}} \right) + y_{H_2}^0 u_{H_2}}{1 + \left(\frac{y_{H_2}^0 u_{H_2}}{2 y_{O_2}^0 u_{O_2}} \right) - \frac{y_{H_2}^0 u_{H_2}}{2}} \tag{A3}$$

This is the final expression for the mole fractions of water in the fuel and air streams exiting the cell. Utilization is the inverses of stoichiometry.

The relative humidity of the exiting gases is:

$$RH_E = \frac{y_w P}{p_{sat}(T_{co})} \tag{A4}$$

where P is the absolute pressure of the gases exiting the stack and the denominator is the saturation pressure of water evaluated at the coolant exit temperature.

The fraction of water exiting as a vapor, f_v, is a more physically meaningful figure of merit than RH_E, when $RH_E > 1$.

$$f_v = \left(\frac{y_{sat}}{1 - y_{sat}} \right) \left(\frac{1 - y_w}{y_w} \right) \tag{A5}$$

The fraction of water exiting the cell as liquid is $f_l = 1 - f_v$.

Appendix B. Conductivity of Nafion

The conductivity of Nafion varies strongly with relative humidity and weakly with temperature over the range of conditions explored in this work. The conductivity, in S cm^{-1}, at 80 °C was fit to the equation:

$$\kappa = 0.0089 \cdot \exp(2.1564 \cdot RH); \quad 0.3 < RH < 1 \tag{B1}$$

References

[1] H.A. Gasteiger, M.F. Mathias, in: M. Murthy, T.F. Fuller, J.W. Van Zee (Eds.), Proceedings of the Symposium on Proton Conducting Membrane Fuel Cells III, The Electrochemical Society Proceedings Series, Pennington, NJ, 2005, pp. 1–24. PV 2002-31.
[2] M.F. Mathias, J. Roth, J. Fleming, W. Lehnert, in: W. Vielstich, H.A. Gasteiger, A. Lamm (Eds.), Handbook of Fuel Cells - Fundamentals, Technology and Applications, vol. 3, John Wiley & Sons, West Sussex, 2003, p. 523.
[3] A.Z. Weber, J. Newman, J. Electrochem. Soc. 153 (2006) A2205–A2214.
[4] S.F. Burlatsky, V.V. Arrazhev, M. Gummalla, D.A. Condit, F. Liu, J. Power Sources 190 (2009) 485–492.
[5] J.P. Owejan, J.E. Owejan, W. Gu, T.A. Trabold, T.W. Tighe, M.F. Mathias, J. Electrochem. Soc. 157 (2010) B1456–B1464.
[6] D.A. Caulk, D.R. Baker, J. Electrochem. Soc. 157 (2010) B1237–B1244.
[7] A.Z. Weber, Electrochim. Acta 54 (2008) 311–315.
[8] M. Khandelwal, M.M. Mench, J. Power Sources 161 (2006) 1106–1115.
[9] O. Berheim, P.J.S. Vie, J.G. Pharoah, S. Kjelstrup, J. Power Sources 195 (2010) 249–256.
[10] F.P. Incopera, D.P. DeWitt, Fundamentals of Heat and Mass Transfer, third ed., John Wiley & Sons, New York, 1990, p. 365.
[11] V.V. Dharaiya, S.G. Kandlikar, J. Heat Transfer 134 (2012) 020911-1–020911-10.
[12] M.J. Martinez, S. Shimpalee, J.W. Van Zee, J. Electrochem. Soc. 156 (2009) B80–B85.
[13] N. Nonoyama, S. Okazaki, A.Z. Weber, Y. Ikogi, T. Yoshida, J. Electrochem. Soc. 158 (2011) B416–B423.
[14] J.C. Slattery, R.B. Bird, AIChE J. 4 (1958) 137–142.
[15] R.C. Reid, J. Prausnitz, T.K. Sherwood, The Properties of Gases and Liquids, McGraw-Hill Inc., New York, 1977.
[16] K. Sakai, K. Sato, T. Mashio, A. Ohma, K. Yamaguchi, K. Shinohara, ECS Trans. 25 (1) (2009) 1193–1201.

Glossary

A: constant in Antoine's equation
B: constant in Antoine's equation
C: constant in Antoine's equation
D: diffusion coefficient
CL: catalyst layer
CP: carbon paper
E: enthalpy voltage
f: fraction
F: Faraday constant
FF: flow field
h: mass-transport coefficient
i: current density
I: current
k: thermal conductivity
κ: conductivity
L: thickness
MPL: microporous layer
n: molar flux
N: molar flow
N_m: MacMullin number
Nu: Nusselt number
p: partial pressure
P: pressure
R: resistance
RH: relative humidity
Sh: Sherwood number
T: temperature
u: utilization
q: heat flux
V: voltage
x: length dimension
y: mole fraction
z: fraction

Subscripts and superscripts
a: air
c: coolant
C: contact
CL: catalyst layer
CP: carbon paper
E: exit
f: fuel
FF: flow field
H: heat
i: component or region
sat: saturation
t: thermal
T: total
v: vapor
w: water
0: inlet